International Journal of Pharmaceutics 380 (2009) 206–215

Contents lists available at ScienceDirect

International Journal of Pharmaceutics

journal homepage: www.elsevier.com/locate/ijpharm

Pharmaceutical Nanotechnology

Nanovesicles released by *Dictyostelium* cells: A potential carrier for drug delivery

Françoise Lavialle[a], Sophie Deshayes[a], Florence Gonnet[b], Eric Larquet[c], Sergei G. Kruglik[a], Nicolas Boisset[c,1], Régis Daniel[b], Annette Alfsen[d], Irène Tatischeff[a,*]

[a] CNRS, UMR7033, Université Pierre et Marie Curie, Laboratoire de Biophysique Moléculaire Cellulaire et Tissulaire, Genopole, F-91030 Evry, France
[b] CNRS, UMR8587, Université Evry val d'Essonne, Laboratoire Analyse et Modélisation pour la Biologie et l'Environnement, F-91025 Evry, France
[c] CNRS, UMR7590, Institut de Minéralogie et de Physique des Milieux Condensés, Université Pierre et Marie Curie, F-75252 Paris, France
[d] CNRS, UMR8104, INSERM, U567, Institut Cochin, Département de Biologie Cellulaire, Université Paris-Descartes, F-75014 Paris, France

ARTICLE INFO

Article history:
Received 23 March 2009
Received in revised form 26 June 2009
Accepted 29 June 2009
Available online 7 July 2009

Keywords:
Extracellular vesicles
Drug delivery
Hypericin
Dictyostelium discoideum

ABSTRACT

Nanovesicles released by *Dictyostelium discoideum* cells grown in the presence of the DNA-specific dye Hoechst 33342 have been previously shown to mediate the transfer of the dye into the nuclei of Hoechst-resistant cells. The present investigation extends this work by conducting experiments in the presence of hypericin, a fluorescent therapeutic photosensitizer assayed for antitumoral photodynamic therapy. Nanovesicles released by *Dictyostelium* cells exhibit an averaged diameter between 50 and 150 nm, as measured by transmission cryoelectron microscopy. A proteomic analysis reveals a predominance of actin and actin-related proteins. The detection of a lysosomal membrane protein (LIMP II) indicates that these vesicles are likely generated in the late endosomal compartment. The use of the hypericin-containing nanovesicles as nanodevices for *in vitro* drug delivery was investigated by fluorescence microscopy. The observed signal was almost exclusively located in the perinuclear area of two human cell lines, skin fibroblasts (HS68) and cervix carcinoma (HeLa) cells. Studies by confocal microscopy with specific markers of cell organelles, provided evidence that hypericin was accumulated in the Golgi apparatus. All these data shed a new light on *in vitro* drug delivery by using cell-released vesicles as carriers.

1. Introduction

Efficient internalization of therapeutic agents within cells is required to successfully achieve both conventional drug mediated-therapy and gene-therapy. The rational for our study is the search for overcoming the general cell resistance towards cell penetration of therapeutic drugs, as previously demonstrated with a DNA-specific drug (Tatischeff et al., 2008).

Besides viral-designed vectors, an assortment of non-viral tools, including liposomes, polymers and nanoparticles, have been proposed to vectorize therapeutic agents both *in vitro* and *in vivo* (Derycke and De Witte, 2002; Torchilin, 2005; Delcayre and Le Pecq, 2006; Weissig et al., 2006). We have previously shown that cells of *Dictyostelium discoideum*, a non-pathogenic eukaryotic amoeba, constitutively release nanovesicles (Tatischeff et al., 1998, 2008). When cell growth is initiated in the presence of exogenous molecules, such as a DNA-specific dye, Hoechst 33342 (HO342), *Dictyostelium* cells produce dye-loaded nanovesicles as a detoxification mechanism (Tatischeff et al., 1998). These nanovesicles can transfer their cargo to the nuclei of naive *Dictyostelium* and human leukeamia K562r resistant cells, which are both resistant to the vital labeling of their nuclei by the dye (Tatischeff et al., 2008). Consequently, we proposed that these nanovesicles of biological origin could also be loaded with therapeutic molecules and then used as a nanodevice for cellular drug internalization.[2]

In the fight against cancer, photodynamic therapy is a non-invasive technique, which involves the systemic administration of a photosensitizer and the local irradiation of the tumor tissue with visible light in order to generate highly cytotoxic reactive oxygen species. Among available photosensitizers, the polycyclic anthraquinone hypericin, a natural pigment present in *Hypericum perforatum* is endowed with promising properties for photodiagnosis and photodynamic therapy of cancer (Agostinis et al., 2002; Head et al., 2006; Ritz et al., 2007; Buytaert et al., 2008; Seitz et al.,

* Corresponding author at: ANBioΦ (BioMoCeTi), CNRS FRE 3207, Université Pierre et Marie Curie, Genopole Campus 1, Bat. Genavenir 8, 5 rue Henri Desbruères, F-91030 Evry Cedex, France. Tel.: +33 1 69 87 43 56; fax: +33 1 69 87 43 60.
E-mail address: irene.tatischeff@upmc.fr (I. Tatischeff).
[1] Deceased on January 2008.

[2] Tatischeff, I., Alfsen, A., Lavialle, F. Extracellular vesicles from non-pathogenic amoeba useful as vehicle for transferring a molecule of interest to an eukaryotic cell. Pending European Patent (UPMC) – Publication No. EP1644045.

0378-5173/$ – see front matter © 2009 Elsevier B.V. All rights reserved.
doi:10.1016/j.ijpharm.2009.06.039

2007, 2008). However, hypericin is a lipophilic non-hydrosoluble drug, making its intraveinous injection problematic (Van De Putte et al., 2006). To overcome this difficulty and to optimize therapeutic effect of the agent, different delivery systems have been developed *in vitro* (see Saw et al., 2006 for review), such as polyvinylpyrrolidone binding, LDL-assisted endocytosis or embedding in sterically stabilised PEG-liposomes (Derycke and De Witte, 2002). When considering *in vivo* applications, the fast elimination of liposomes from the blood has been overcome by different sterical stabilizations (Torchilin, 2005). However, some drawbacks of the carrier-systems remain, such as the loss of substantial amount of hypericin from the liposomes (Derycke and De Witte, 2002), followed by potential harmful aggregation in physiological media.

In our study, hypericin was chosen as an antitumoral compound of interest to promote the nanovesicles released by *Dictyostelium* cells as drug carriers. After studying the loading capacity of these nanovesicles with the hydrophobic photosensitizer, an *in vitro* vesicle-mediated hypericin transfer assay was successfully conducted on two human cell lines, HS68 skin fibroblasts and carcinomic HeLa cells. The results point out the vesicles from *Dictyostelium* cells as a new interesting bio-engineered carrier device for drug delivery.

2. Materials and methods

If not otherwise specified, chemical reagents were from Sigma (L'Isle d'Abeau Chesnes, France) of the highest available purity.

2.1. Cell cultures

Dictyostelium cells (http://www.dictybase.org), Ax-2 strain, were grown in suspension in the dark, on a gyratory shaker (150 rpm) at +22 °C, in HL5 semi-defined medium (Sussman, 1987) containing penicillin (50 U/mL) and streptomycin (50 μg/mL) (Biomedia, Boussens, France).

HS 68 cells (American Type Culture Collection, Rockville, MD, USA) and HeLa cells (American Type Culture Collection, Manassas, VA, USA) were seeded at 5×10^5 cells/mL (2 mL) on glass coverslips deposited in 35-mm culture dishes (Becton Dickinson, Le Pont de Chaix, France). Cells were grown in DMEM supplemented with 10% (v/v) fetal-calf serum, at 37 °C, in a humidified atmosphere with 5% CO_2.

2.2. Production of nanovesicles

Dictyostelium cells were grown in HL5 (50 mL) in the absence (control) or in the presence of hypericin (Molecular Probes, Invitrogen, Cergy-Pontoise, France), at a final concentration of 25 μM (313 μL of a 4 mM stock solution in DMSO added to the cell suspension). After 48 h of growth, cell suspensions were centrifuged at 700 × *g* for 5 min (+22 °C). 45 mL of the cell-free medium were centrifuged at 2000 × *g* for 10 min (+22 °C). 40 mL of the 2000 × *g* supernatant was centrifuged at 12,000 × *g* for 30 min (+4 °C). Nanovesicles present in the pellets were resuspended in 400 μL of phosphate buffered saline (PBS), pH 7.2 without calcium and magnesium (GIBCO). For proteomic analysis, an additional centrifugation at 12,000 × *g* was carried out.

The protein concentration of each of the seven preparations of nanovesicles was measured by the method of Peterson (Peterson, 1977). It ranged from 1.9 to 2.6 mg/mL. These nanovesicles were quite stable in PBS, as they did withstand repeated liquid nitrogen freeze–thaw cycles without breaking. Their *in vitro* long-term stability in PBS at 4 °C was controlled periodically by fluorescence spectroscopy (see Section 2.5). As observed with HO342, they could be kept at +4 °C at least 2 months without releasing the dye.

2.3. Transmission cryoelectron microscopy

A 5 μL droplet of the vesicle suspension was applied to a 400-mesh copper grid, coated with a thin holey-carbon film. Excess of solution was removed with Whatman paper and the grid was rapidly plunged into liquid ethane (Taylor and Glaeser, 1974; Dubochet, 2007) and transferred under liquid nitrogen into the microscope using a side entry nitrogen-cooled Gatan 626 cryoholder. Sample analysis was carried out under a JEOL JEM 2100F transmission cryoelectron microscope with an acceleration voltage of 200 kV, a nominal magnification of 54,804× estimated with tobacco mosaic virus as reference (Boisset and Mouche, 2000) and defocus ranging from −1.7 to −3.2 μm, accurately determined using enhanced power spectra (Jonic et al., 2007). Images were recorded under low dose conditions (10 electrons per A^2) with a 4k × 4k Gatan Utrascan CCD camera.

2.4. Proteomics

2.4.1. In gel digestion

After separation of vesicle proteins on 10% SDS-PAGE, 19 discrete Coomassie-stained bands were excised from the gel. The in-gel digestion was carried out using porcine trypsin from Promega, France. Briefly, gel pieces (in 0.5 mL BioPure, Eppendorf) were rinsed with 400 μL of pure acetonitrile and placed for 5 min in an ultrasonic bath. After removal of the solvent, each dehydrated gel piece was then rehydrated with 40 μL of 30 mM ammonium hydrogen carbonate containing 0.4 μg of trypsin. The digestion was carried out at 37 °C for 6 h. Supernatants were collected and the gel pieces were first washed with 40 μL 1% formic acid (5 min in the ultrasonic bath) and then with 50 μL 100% acetonitrile (5 min in the ultrasonic bath). All supernatants (from each fraction) were pooled and evaporated under vacuum (SpeedVac). The extracted peptides were then resuspended in 10 μL 1% formic acid, and were directly extracted/concentrated using C18 ZipTip pipette tips (Millipore), washed with 1% formic acid and eluted with 1.5 μL of α-cyano-4-hydroxycinnamic acid at 3.3 μg/μL in 80% acetonitrile/1% formic acid.

2.4.2. Mass spectrometry and database query

The total peptide eluate (1.5 μL) was applied dropwise onto a MALDI target plate. MALDI-TOF mass spectrometry was performed on a Voyager-DE STR™ (Applied Biosystems). All spectra were acquired in a positive reflector mode (20 kV accelerating voltage) with 225 ns delayed extraction. Typically 200 shots were recorded per sample from different crystals on the MALDI target, 50 shots per crystal. Trypsin autolytic peptides were used to internally calibrate each deisotoped spectrum to a mass accuracy within 20 ppm. Peak lists were generated by Data Explorer software (Applied Biosystems, version 4.0.0.0 of 18 October 2000). After calibration, peptide mass list was filtered for trypsin autolytic peptides and keratins (if any). Tryptic monoisotopic peptide masses were searched by using Aldente software (version 11/09/2006) (http://www.expasy.org/tools/aldente) in the UniProtKB/Swiss-Prot database (Release 51.5 of 23 January 2007, 265,198 protein entries) and UniProtKB/TrEMBL database (Release 34.5 of 23 January 2007, 3658,674 protein entries) with the following parameters: *D. discoideum* species, one missed cleavage site and mass tolerance setting of 20 ppm. Partial chemical modification such as oxidation of methionine was taken into consideration for the queries. Identification with the highest confidence are based on statistically significant search scores, and are consistent with the gel region from which the protein was excised (MW) and account for the extent of sequence coverage and the number of peptides matched (minimum of 4). Only proteins with the highest statistical search scores are presented in the study herein. When two proteins

of similar MW are identified with nearly the same probability, both are reported.

2.5. Fluorescence spectroscopy

Fluorescence emission spectra were recorded with an Aminco. Bowman Series 2 Luminescence spectrometer, using a (2 mm × 10 mm) quartz cuvet (Hellma France, Paris). All fluorescence measurements were made at +20 °C. Vesicles were diluted in PBS (1/25) and characterized by their tryptophan fluorescence emission spectra, obtained with 280 nm excitation. The grating second order of Rayleigh diffusion of the 280 nm excitation wavelength was measured at 560 nm and used as a marker of diffusing components, namely the vesicles. Hypericin florescence emission spectra were measured with 545 nm excitation. Hypericin content of each preparation of nanovesicles obtained from cells grown in the presence of the drug was calculated from the fluorescence intensity measured at 590 nm with a fixed 545 nm excitation wavelength. Samples containing 120 μL of nanovesicles in PBS (protein concentration 0.10 mg/mL) were analyzed after addition of 120 μL of ethanol. A calibration curve was constructed using hypericin samples at final concentrations <2.5 μM in PBS:ethanol 1:1 (v/v). Noteworthy, the calibration curve was no more linear for higher hypericin concentrations, due to the very low Stockes shift between absorption and fluorescence emission spectra. The presence of ethanol was required to disrupt the vesicles and to solubilize hypericin in its fluorescent monomeric form.

2.6. Flow cytometry

Cell suspensions fixed in paraformaldehyde 2% final concentration in PBS were analyzed at approximately 2×10^6 cells/mL using a Beckton Dickinson FACSCalibur 3C flow cytometer (argon laser at 488 nm). Cells (10^4) were analyzed for side (SSC)- and forward (FSC)-light scattering and for FL2-fluorescence. The kinetics of hypericin internalization in *Dictyostelium* cells was obtained from the mean FL2-fluorescence intensity measured as a function of incubation time.

2.7. Video-microscopy

HS68 and HeLa cells cultured on glass coverslips were first rinsed with DMEM without fetal-calf serum and then incubated in the dark, at 37 °C, in a humidified atmosphere with 5% CO_2, either in the presence of 50 μL of hypericin-loaded nanovesicles (protein concentration 0.21 mg/mL in PBS) inholding 7 μM hypericin, for 1 h, or with 7 μM hypericin dispersed in DMEM (from a stock solution at 4 mM in DMSO) for 30 min. Cells were rinsed with DMEM without fetal-calf serum, and observed under an Olympus BHA transmission microscope (Olympus France, Rungis) equipped with a 100 W mercury lamp and a blue fluorescence excitation block. Images were collected by a home-made video setup and a black and white analogical CCD camera. Data acquisition was achieved using NIH Image 1.63.

2.8. Confocal fluorescence microscopy

HS68 and HeLa cells cultured on glass coverslips were rinsed with DMEM without fetal-calf serum and incubated for 30 min in the dark, at 37 °C in a humidified atmosphere with 5% CO_2 in the presence of nanovesicles loaded with 7 μM hypericin. A Golgi marker (BODIPY FL C5-ceramide, Molecular probes, Invitrogen, Cergy-Pontoise, France), at 15 μM final concentration in DMEM was then added. Cell labeling lasted for another 30 min at 37 °C in the dark. Cells were rinsed with DMEM without fetal-calf serum before observation. In experiments carried out with a lysosome marker, 0.5 μM LysoTracker Green (Molecular probes, Invitrogen, Cergy-Pontoise, France), cells were rinsed with DMEM and incubated for 60 min in the dark at 37 °C in a humidified atmosphere with 7% CO_2, with both the hypericin-loaded nanovesicles and the lysosome marker. Cells were rinsed with DMEM without fetal-calf serum before observation.

Confocal fluorescence microscopy imaging was performed using a confocal laser scanning microscope (model LSM 510, Carl Zeiss, Jena, Germany) equipped with an Argon laser 25 mW (laser excitation sources at 488 and 533 nm) using a 63 × 1.4 NA-Plan-Apochromat oil immersion objective.

2.9. Confocal Raman spectroscopy

The Raman spectrum of vesicles (100 μL at a protein concentration of 1.25 mg/mL) has been recorded using a home-built Raman setup. Excitation light at 780 nm was provided by a continuous-wave Ti:sapphire laser (Spectra Physics, model 3900S) pumped by an argon-ion laser (Spectra Physics Stabilite 2017). Excitation power was attenuated by a neutral density filter to 60 mW in the sample compartment. Laser light was focused into the sample by a water-immersion infinity-corrected objective (Olympus LUMFL 60×, NA = 1.1), which also collected the Raman signal and delivered it onto the spectrograph (Acton SpectraPro 2500i) coupled with a deep-depletion back-illuminated CCD camera (Princeton Instruments SPEC-10 400BR/LN). Confocal detection was achieved by insertion of a 50-μm pinhole at the position of the spectrograph entrance slit; Raman light was focused into the pinhole by an achromatic lens with f = 75 mm. Spatial lateral resolution was estimated to be ~0.6 μm. Raman signal was separated from laser light by two Semrock RazorEdge long pass filters (grade "U"). One filter, with λ_{laser} = 780 nm, was placed perpendicularly to the optical beam just before the focusing lens; another one, with λ_{laser} = 830 nm, was used as a dichroic beamsplitter at an angle of incidence 45°: it reflected laser light at 780 nm and transmitted all the wavelengths longer than 785 nm. Raman spectra were acquired with WinSpec software; further treatment was performed using Igor Pro for Windows software. Among the 200 spectra accumulated with an exposure time of 5 s each, 70 spectra exhibiting the lowest background were selected and averaged. The resulting spectra were then corrected for the signal originating from PBS, glass substrate and all the optical elements located along the detection pathway. Bands were assigned according to published data (Notingher et al., 2003; Uzunbajakava et al., 2003; Krafft et al., 2006).

2.10. Hypericin cytotoxicity assessment

In the present work, the photodynamic efficiency of hypericin on HeLa cells was measured using a viability (MTT) test (Zhang et al., 1995). HeLa cells were seeded at 10^5 cells per well in 96-well flat-bottom plates and cultivated for 48 h at 37 °C in DMEM supplemented with 10% fetal-calf serum (FCS) in a 5% CO_2 atmosphere. Prior irradiation, cells were washed with PBS and then incubated for 1 h at 37 °C in a CO_2 atmosphere either in the presence of free hypericin (2% DMSO) or in the presence of nanovesicles loaded with hypericin. Hypericin final concentration ranged from 0.25 to 7 μM for free hypericin and from 0.25 to 2.5 μM for vesicular hypericin. After incubation, cells were washed with PBS and DMEM supplemented with 10% FCS was added. Irradiations were carried out using a 300 W Xenon arc mounted in a lamp housing equipped with a rear reflector and a 3 in. diameter fused silica condenser of f/0.7 aperture (Oriel, Statford, CT). After elimination of infrared light by a water filter (8 cm), the beam was passed through an interference filter centered at 600 nm with a half bandwidth of 30 nm (K60 from Balzers, Liechtenstein). The exit beam was reflected to the bottom by a 45° mirror to allow irradiation of the samples contained in a 96-well flat-bottom plate. The uniformity of light intensity was

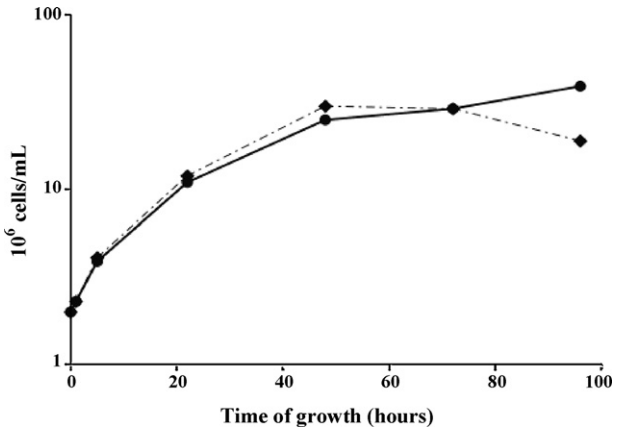

Fig. 1. *Dictyostelium* cell growth in the absence and in the presence of hypericin 25 μM. Cell cultures were initiated at 5×10^5 cells/mL in the absence (●) or in the presence (♦) of hypericin. At the indicated times, cells were counted using a Bürker hemocytometer. The curve shows a representative kinetics.

controlled by scanning the working area with a power meter (Scientech, Boulder, CO), typical light intensities were 6.7 mW/cm^2. The diameter of the incident beam on the 96-well plate was about 5 cm. Irradiation times were 5 or 10 min. In each experiment, a light positive control without hypericin as well as dark controls (with and without hypericin) were included. MTT assays were performed 24 h following irradiation. Cells were washed with PBS and incubated in the presence of 100 μL of MTT salts (2 mg/mL, Sigma–Aldrich) for additional 5 h at 37 °C. Addition of 100 μL of DMSO allowed dissolving the insoluble formazan product, correlated to the relative viable cell number. The absorbance (A), corresponding to the solubilized formazan pellet, was measured at 570 nm using a Labsystems Multiscan MS microplate reader. Blank values measured in wells without cells were subtracted. Dark controls served as 100% viability values.

3. Results

3.1. *Dictyostelium* cells produce nanovesicles loaded with hypericin

Dictyostelium cells are capable to internalize exogenous molecules and to get rid of them as cargo molecules packaged into nanovesicles released in the external medium. With the aim to use these nanovesicles as a vector for therapeutic drugs, we carried out assays with hypericin, a promising photosensitizer for phototherapy. If light-dependent toxicity of hypericin is well known (Ritz et al., 2007; Wielgus et al., 2007), the molecule has also been suggested to have noticeable cytotoxic effects in the absence of light (Blank et al., 2001). Therefore, we checked that the photosensitizer did not affect the cell growth in our experimental conditions (Fig. 1). In control conditions (i.e. in the absence of hypericin), the cell density doubles about every 12 h. After 48 h, as the cell density reaches 2×10^7 cells per mL, the growth rate decreases probing that cells enter the so-called stationary phase. A similar kinetics of growth was observed for cells cultivated in the presence of 25 μM hypericin, at least up to 72 h. In parallel, the cell morphology was checked by flow cytometry from dot-plots constructed by plotting the intensity of light diffusion measured at large angles (SSC) against the intensity of light diffusion at small angles (FSC), i.e. probing cell vacuolization and cell size, respectively. Data shown in Fig. 2A indicate that hypericin does not significantly modify the cell morphology up to a 48-h incubation period. After a 72-h incubation period, the cell size decreases, likely as a result of ini-

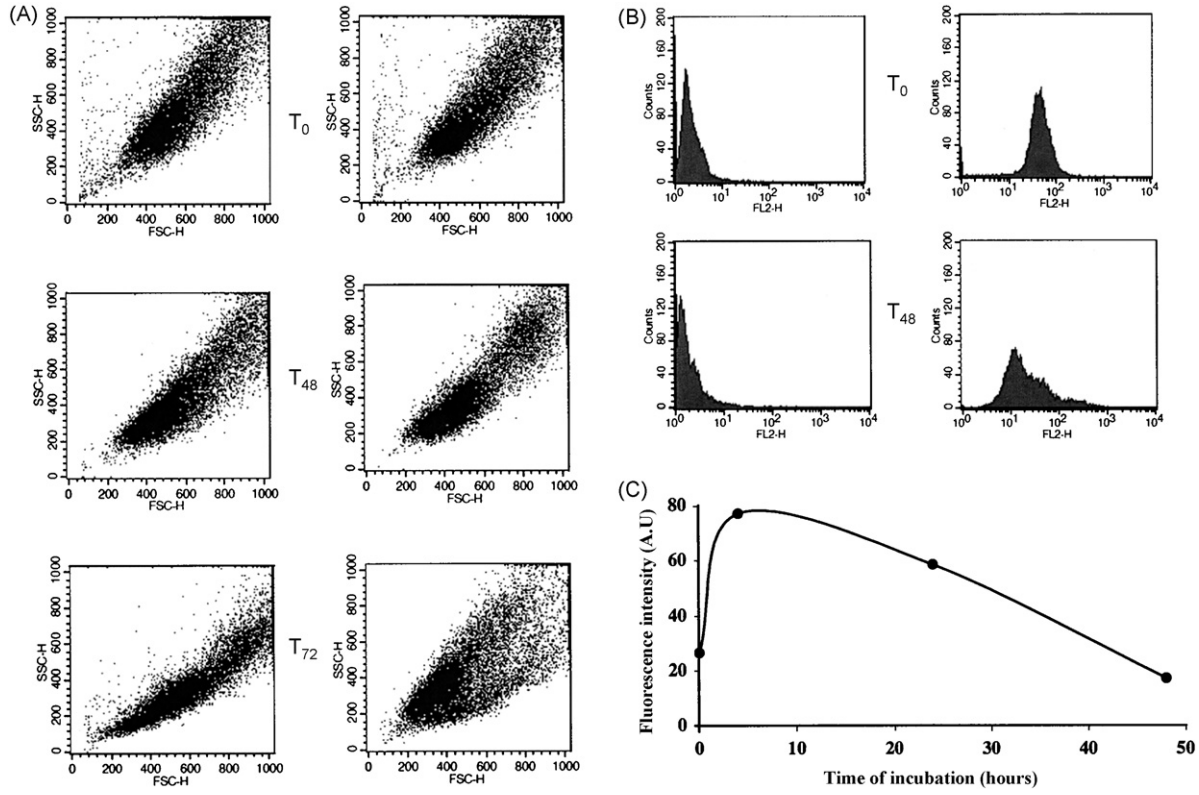

Fig. 2. FACS analysis of hypericin internalization within *Dictyostelium* cells. Aliquots of cells grown in the absence or in the presence of 25 μM hypericin were fixed in PFA 2% at given times of growth (4, 24, 48 and 72 h). (A) (SSC–FSC) dot-plots of cells grown in the absence (left column) and in the presence of hypericin (right column). Times of sampling: T_0, $T_{48\,h}$ and $T_{72\,h}$. (B) FL2-fluorescence associated to *Dictyostelium* cells grown in the absence (left column) or in the presence of hypericin (right column). Times of sampling: T_0 and $T_{48\,h}$. (C) Kinetics of *Dictyostelium* cell labeling. The graph was constructed from the mean FL2-fluorescence intensities of cells incubated for 0, 4, 24 and 48 h in the presence hypericin (the corresponding mean FL2-fluorescence intensities of control cells was subtracted).

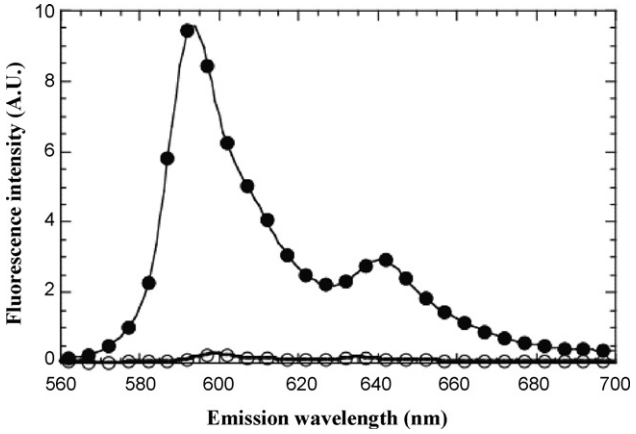

Fig. 3. Spectrofluorimetric detection of hypericin packaged within nanovesicles. Fluorescence emission spectra of hypericin packaged in nanovesicles, released by *Dictyostelium* cells grown for 48 h in the presence of 25 μM hypericin. Excitation wavelength was fixed at 545 nm. (○) nanovesicles in PBS and (●) nanovesicles in PBS:ethanol 1:1 (v/v).

tiation of apoptosis. Accordingly, cell cultures were conducted in the presence of 25 μM hypericin during 48 h. Flow-cytometry measurements also supply informations upon hypericin accumulation within *Dictyostelium* cells. According to Fig. 2B, a significant fluorescent signal assigned to cellular autofluorescence was detected in cells grown in the absence of hypericin. After addition of 25 μM hypericin in the growth medium (T_0), the FL2-fluorescence intensity of the cells immediately increased (notice the log scale), and decrease after 48 h. According to Fig. 2C, after a 4-h incubation, the mean FL2-fluorescence intensity increased from 26 to about 80 arbitrary units (A.U.). Then, the fluorescence intensity dropped to 60 A.U. and to 23 A.U., after 24 and 48 h, respectively, in the presence of hypericin. As observed previously with HO342 (Tatischeff et al., 1998, 2008), the kinetics of cell labeling might fit the following scenario: *Dictyostelium* cells internalize hypericin and then, get rid of it associated to nanovesicles released in the culture medium. This hypothesis was tested by analyzing vesicles released by cells incubated for 4, 24 and 48 h in the presence of 25 μM hypericin. No significant hypericin fluorescence was detected in vesicles prepared from cell cultures incubated with the drug for 4 and 24 h. By contrast, a fluorescent signal characteristic of hypericin was observed with vesicles released by cells after a 48-h incubation period. The low fluorescence emission of hypericin-associated nanovesicles in PBS was greatly intensified by means of ethanol disruption of the vesicles and further solubilization of their hypericin content (Fig. 3).

Efficiency of the loading process was approached by studying vesicles released by cells incubated for 48 h in the presence of either 5, 10 or 25 μM hypericin. Hypericin quantification indicates that these nanovesicles were, respectively, loaded with 22, 54 and 64 μM hypericin. The efficiency of this cell-mediated labeling of vesicles was stressed by testing a direct labeling procedure. Such «exogenous» labeling was attempted by incubating control vesicles for 30 mn at 21 °C in the presence of 25 μM hypericin in PBS (stock solution, 4 mM in DMSO). The presence of hypericin aggregates cosedimenting with the vesicles prevented the use of this labeling method.

3.2. Morphological, spectral and proteomic characterization of the nanovesicles

Morphological analysis of vesicles prepared from the growth medium of cells cultivated in the absence or in the presence of 25 μM hypericin was carried out by cryoelectron microscopy imaging. Two parallel dark lines imaging the lipid membrane bilayer that delineates the vesicles are quite visible in Fig. 4. No difference in shape was observed between vesicles prepared from control and hypericin-exposed cell cultures, both appearing mostly smooth and round. The histogram of size distribution computed on 59 vesicles, prepared in the absence of hypericin, clearly indicates that almost 80% of them have an average diameter within a range of 50–150 nm (Fig. 4E). Such a size heterogeneity has previously been reported for exosomes originating from leukemia cells (Laulagnier et al., 2005). Interestingly, some vesicles seem to be filled with dense granular material, while others appear almost empty (Fig. 4A and D), as already observed by transmission electron microscopy after negative staining (Tatischeff et al., 2008).

The chemical composition of the nanovesicles was studied by Raman spectroscopy (Fig. 5). As expected, a large contribution from lipids can be distinguished. Characteristic spectral range around 1100 cm^{-1} contains pronounced C–C stretch bands at ~1063, ~1085 and ~1125 cm^{-1}, in good agreement with earlier Raman study of bilayer systems (Lavialle and Levin, 1980; Cherney et al., 2003). Additional signals characteristic of lipids are detected at ~1296 and ~1441 cm^{-1}. Raman signatures of proteins can be easily discerned in Fig. 5, as illustrated by the signal at ~1450 cm^{-1}. The intensity of this protein signal is insensitive to protein secondary structure and depends only on the number of protein CH_2 and CH_3 groups. Amide I band at ~1656 cm^{-1} and Amide III band at ~1257 cm^{-1} are also significant, as well as the phenylalanine ring breathing mode at ~1002 cm^{-1}. The Raman band around 782 cm^{-1} is a well-known nucleotide marker band, to which a number of vibrational modes contribute. Most dominant contributions are from the complex vibration of the 5′C–O–P–O–C3′ network (Deng et al., 1999) and the cytosine ring breathing mode. Thymine and uracil bases identifying DNA and RNA, respectively, also may contribute to this band. In fact, since the well-known Raman marker band for A-type helices in RNA located at 813 cm^{-1} is absent, we conclude that the band at 782 cm^{-1} is mainly due to contribution of DNA. The DNA Raman bands observed at ~1094 and ~1575 cm^{-1} strongly support this conclusion.

If Raman spectroscopic mapping nowadays enables to study the chemical composition and molecular structure of subcellular components in individual cells without the need of labeling, only few Raman studies on the vibrational characteristics of extracellular vesicles components have been published yet (Ajito and Torimitsu, 2002). Of special interest is the evidence for the presence of DNA, supporting our previous observations (Tatischeff et al., 1998).

For sake of comparison with previous reported proteomic studies of other cell-released vesicles, such as exosomes (Simpson et al., 2008; Mathias et al., 2009), determination of the proteins associated to the nanovesicles was carried by gel electrophoresis and mass spectrometry analysis. 1D-electrophoresis was performed (data not shown) to avoid possible precipitation of membrane proteins upon the isoelectrofocusing separation in 2D gel. SDS-PAGE analysis revealed a rather small number of Coomassie Blue-stained bands as compared to mammalian cells exosomes (Wubbolts et al., 2003; Simpson et al., 2008; Mathias et al., 2009). Proteins for which a minimum of four peptides matching with known *D. discoideum* proteins were listed in Table 1. Among 17 proteins identified, the predominance of 7 actin and actin-related proteins is noteworthy. These cytoplasmic proteins–actin (Swissprot accession P07830), heat shock cognate protein (P36415), actin-related protein 2/3 complex subunit 2, p34-Arc and p-20-Arc (O96623 and O96625, respectively), coronin (P27133), cortexillin (O15813), are all involved in the cellular dynamics and motility. Another interesting point is the detection of small proteins acting as modulators or transducers in transmembrane signaling systems: guanine nucleotide-binding protein subunit beta (P36408), ras-like proteins (P15064 and P32253), adenylyl cyclase-associated protein (P54654), involved in microfilament reorganization near

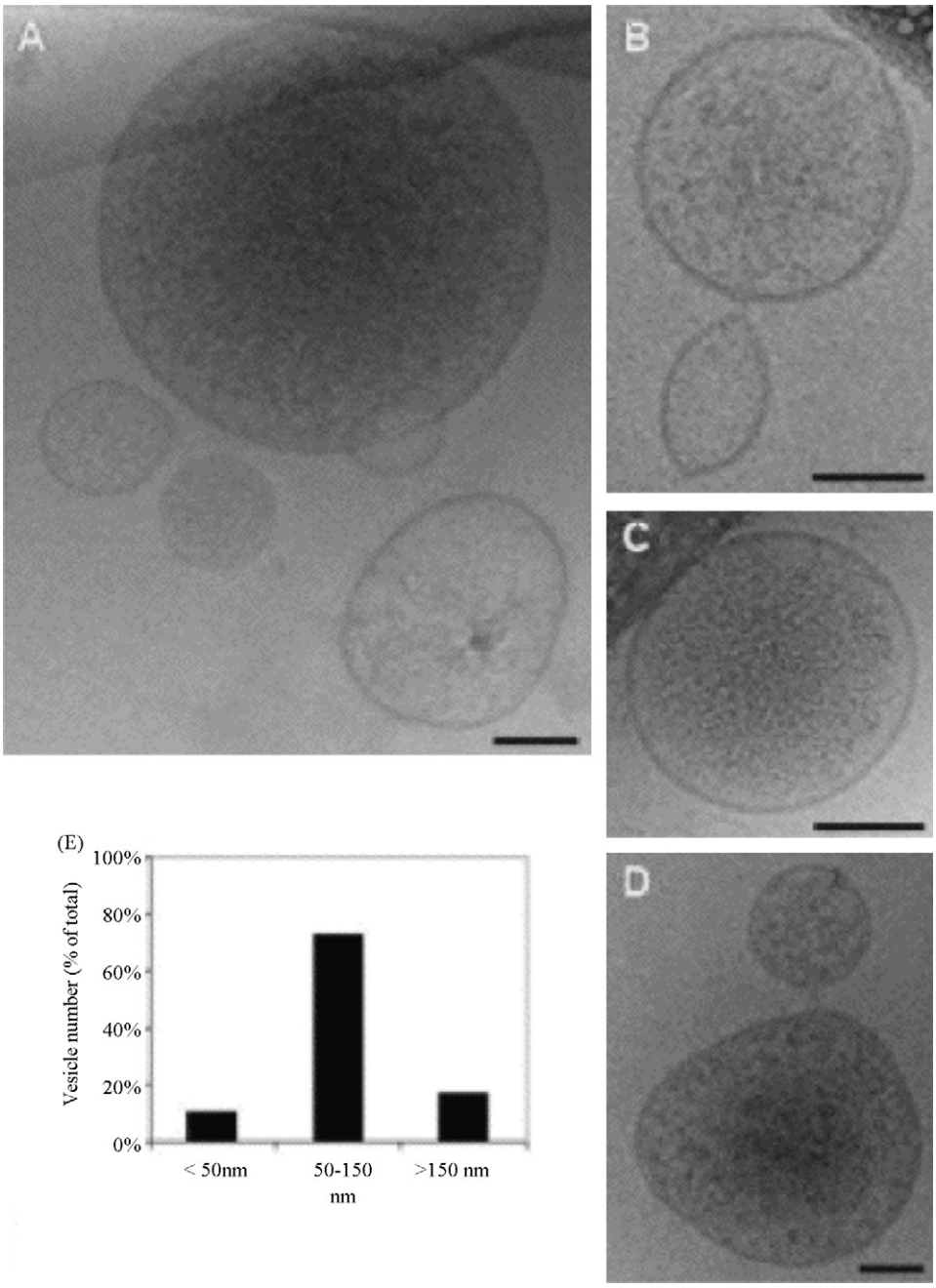

Fig. 4. Morphological characterization of the nanovesicles by cryoelectron microscopy. (A–D) Typical frozen-hydrated nanovesicles, exemplifying their heterogeneity in size (E) Histogram of vesicle size distribution constructed from a set of 59 control vesicles observed in different fields. Bar: 50 nm.

the plasma membrane, and the beta subunit of mitochondria processing peptidase (Q4W6B5). Also to be noted is the membrane proximal localization and lipid-anchoring of most of the proteins unrelated to actin and the transmembrane location of the lysosomal integral membrane protein II (LIMP II or LGP85). The detected lectins, discoidin-1 (C and B chains) and discoidin-2 have been described to play a role in cytoskeletal architecture (Alexander et al., 1992).

3.3. Nanovesicles transfer hypericin to the Golgi apparatus of target cells

Hypericin transfer to target cells was first visualized using human fibroblasts (HS68) as control cells and with HeLa cells used as a model of tumoral cells (Fig. 6). After a 1-h incubation in the presence of hypericin packaged in nanovesicles, a fluorescent signal was detected almost exclusively in the perinuclear area. Under these experimental conditions, neither the cell plasma membrane nor the nucleus was labelled by the hydrophobic cargo molecule. Similar experiments were conducted using free hypericin, i.e. not encapsulated in vesicles, for comparison. After only a 30-min incubation, HeLa cells became round-shaped, the typical morphology of dying cells that have lost their adhesion properties. Loss of cell adhesion has also been reported in the case of zinc(II)–phtalatecyanine-induced photodamage (Galaz et al., 2005). This result demonstrates that the nanovesicles vectorize significant amounts of drug, but also prevent the uncontrolled cell death triggered by free hypericin under the blue light used for observation.

To obtain direct evidence for the intracellular localization of hypericin delivered by the nanovesicles into HeLa target cells,

Table 1
Proteins from *Dictyostelium discoideum* nanovesicles identified by MALDI–TOF-MS.

Band no.	Protein name (SWISS-Prot accession no.)	Theoretical MW (kDa)/p*I*	Sequence coverage/no. of peptides matched	Score	*Z*-Score
Actin					
10	Actin (P02577) or Actin-15 (P07830)	42/5.2	50/14	29.70	11,253.7
Actin polymerization					
6	Heat shock cognate protein (P36415)	70/5.4	15/7	5.43	168.8
14	Actin-related protein 2/3 complex subunit 2, P34-Arc (O96623)	33/9.1	19/5	0.44	43.5
18	P20-Arc (O96625)	20/9.3	21/4	3.08	344.4
Actin filament binding					
8	Coronin (P27133)	49/7.1	11/5	1.86	48.1
8	Cortexillin I (O15813)	51/6.0	16/6	2.08	36.8
Galactose-binding lectin					
14	Discoidin I, C chain and B chain (P02887)	28/6.6	34/7	5.04	526.5
15	Discoidin-2 (P42530)	29/6.7	31/5	1.38	130.5
Ras protein					
16	Ras-like protein rasG (P15064)	21/5.4	29/5	4.90	123.5
16	Ras-related protein Rap-1 (P18613)	21/5.6	19/4	1.40	83.4
16	Ras-like protein rasC (P32253)	21/6.4	28/4	1.03	129.0
Membrane protein					
5	Lysosomal integral membrane protein II (Q9BKJ9)	83/5.1	18/9	11.27	1279.0
Others					
8	Adenylyl cyclase-associated protein (P54654)	50/7.0	14/5	1.55	35.3
9	Beta subunit of mitochondrial processing peptidase (Q4W6B5)	53/5.3	27/8	4.76	634.0
12	Guanine nucleotide-binding protein subunit beta (P36408)	39/6.3	11/5	1.41	122.8
16	Calcium-dependent cell adhesion molecule 1 (P54657)	24/5.4	42/6	4.71	175.8
17	40S Ribosomal protein S9 (P14132)	21/10.5	19/4	1.91	0.0

co-localization studies were performed with fluorescent markers of the Golgi apparatus (BODIPY ceramide) and of lysosomes (LysoTracker). Representative confocal micrographs of the double-stained cells provides evidence that within 1 h, hypericin co-accumulates with BODIPY in the Golgi apparatus (Fig. 7A). By contrast, hypericin and LysoTracker do not co-localize as illustrated by the merged fluorescence image shown in Fig. 7B, indicating that the photosensitizer is not directed to these acidic organelles. These data are in agreement with results obtained by other groups on HeLa cells (Delaey et al., 2001), as well as on glioblastoma and carcinoma cells (Teiten et al., 2003; Uzdensky et al., 2003; Ritz et al., 2007).

3.4. Hypericin-loaded nanovesicles are efficient for photodynamic killing of HeLa cells

Fig. 8 shows that, in the chosen experimental conditions, 1 μM free hypericin induced significant HeLa cell mortality (50%). In the presence of 7 μM free hypericin, cell mortality was close to 80%. Up to 2.5 μM final concentration in hypericin, a similar phototoxicity was obtained using hypericin-loaded nanovesicles.

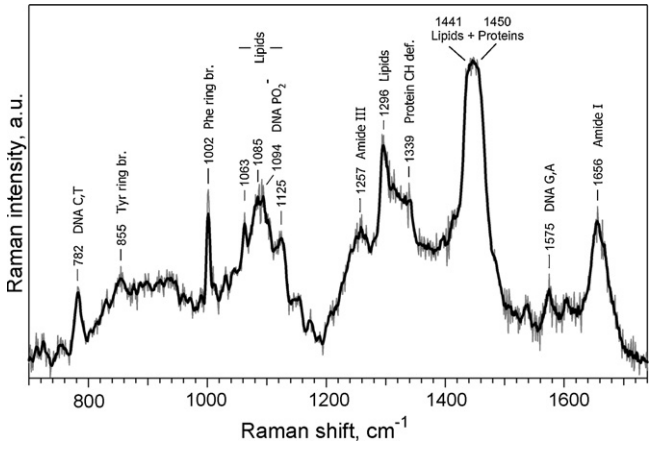

Fig. 5. Raman spectroscopic analysis of the nanovesicles. The vesicle suspension (protein concentration 1.25 mg/mL) was analyzed under the following experimental conditions: excitation wavelength: 780 nm, laser power: 60 mW, 5-s exposure time for each spectrum, average of 70 spectra.

4. Discussion

The present study was initiated to investigate the potential use of *Dictyostelium* cell-released nanovesicles as *in vitro* drug carriers for cancer therapy. It extends our previous investigation using HO342-loaded nanovesicles, that allowed to label the nuclei of naive *Dictyostelium* cells and human leukaemic K562r cells, even though these two cell types are constitutively resistant to the vital staining of their nuclei (Tatischeff et al., 2008). The present results indicate that *Dictyostelium* cells are also able to release into the culture medium nanovesicles loaded with hypericin, a photosensitizer differing in charge and hydrophobicity from the DNA marker. Additionally, these nanovesicles were shown to label human HS68 and HeLa cells. It is worth stressing that the two cargo molecules, HO342 and hypericin, were transferred to two distinct intracellular locations, namely, the nucleus for HO342 and the Golgi apparatus for hypericin. This observation cannot be further explained. It has been previously reported that many mammalian eukaryotic cells, including B lymphocytes, platelets, reticulocytes, K562 cells, dendritic cells and intestinal epithelial cells, release in their extracellular environment, not only soluble proteins and mediators but also vesicles with a lipid bilayer, originating either from the cell surface or from intracellular compartments (Heijnen et al., 1999; Stoorvogel et al., 2002; Thery et al., 2002; Hugel et al., 2005). Designed as microvesicles and/or exosomes, these membrane vesicles are most often released upon cell stimulation, although they can also be secreted in a constitutive manner, i.e. in the absence of any identified stimulus, by intestinal epithelial cells (van Niel et al., 2001) and *Dictyostelium* cells (Tatischeff et al., 1998). According to the literature, exosomes originate in the late endosomal compartment by inward budding of the endosomal membrane, thereby generating multivesicular bodies which fuse with the plasma membrane for releasing extracellularly their vesicles (Stoorvogel et al., 2002; Thery et al., 2002). Interestingly, multivesicular bodies as well

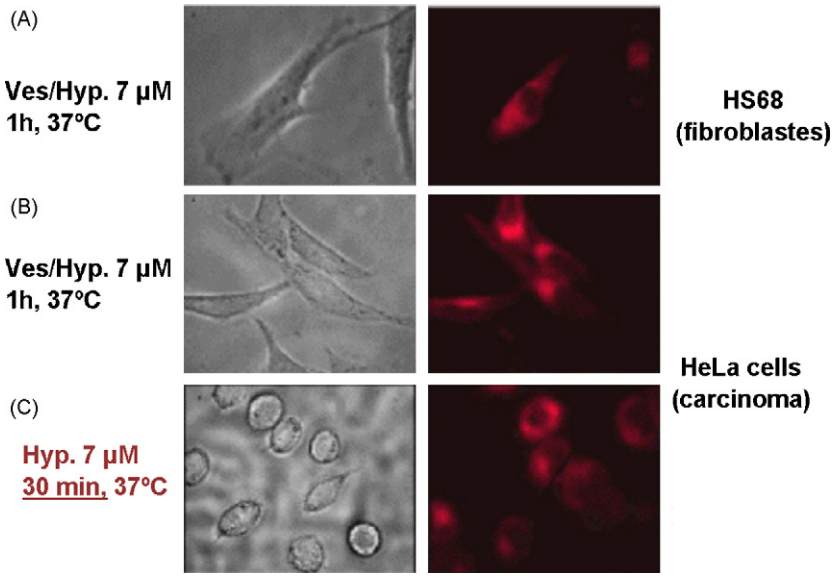

Fig. 6. Light-transmission and fluorescence microscopy of hypericin internalization within target cells. Human fibroblasts (HS68) (A) and HeLa cells (B and C) were incubated at 37 °C in the dark for the indicated times, in the presence of 7 µM hypericin packaged within nanovesicles (A and B) or free in DMEM (C). (For interpretation of the references to colour in this figure legend, the reader is referred to the web version of this article.)

as post-lysosomal secretory granules are known to be present in *Dictyostelium* cells (Neuhaus et al., 2002; Marchetti et al., 2004).

Proteomic studies in mammalian exosomes showed that both membrane proteins and cytoplasmic proteins, such as actin and actin-binding proteins, heat shock proteins (hsp70) and G-proteins were detected (Thery et al., 2002; Wubbolts et al., 2003). The current proteomic investigation reveals that actin and actin-related proteins are major constituents of the nanovesicles released by *Dictyostelium* cells. It favors a link with intracellular trafficking and does not fit with the hypothesis that nanovesicles arise by shedding from the plasma membrane (Heijnen et al., 1999). The current study also reveals the presence of the lysosomal integral membrane protein II, a protein component of the degradation pathway that involves multivesicular bodies (Janssen et al., 2001). This glycoprotein, belonging to the CD36 family, is part of a class of scavenger receptors. Its role in signal transduction linked to cell adhesion suggested that it could be involved in the biogenesis and maintenance of endosomal and lysosomal morphology (Kuronita et al., 2002, 2005). Moreover, we showed previously that lyso-bisphosphatidic acid was present in *Dictyostelium* vesicles (Tatischeff et al., 1998). Noteworthy, this unusual phospholipid is a major membrane constituent of the internal vesicles of multivesicular bodies (Yorikawa et al., 2005). Altogether, these observations strengthen the hypothesis of a multivesicular origin for the nanovesicles released by *Dictyostelium* cells.

The biological mechanism used by *Dictyostelium* cells for loading the nanovesicles with hypericin is yet unknown. Both membrane-solubilized monomers and aggregates of hypericin might be internalized by the cells. As probed by the strong fluorescent signal detected by flow cytometry at the very beginning of the experiment (Fig. 2B), hypericin aggregates rapidly dissociate, at least partially, in the presence of *Dictyostelium* cells. The fluorescent monomeric form of hypericin might follow the endocytosis pathway. Hypericin aggregates, which are present in the culture medium throughout the whole incubation time with the cells, might also be internalized by macro-pinocytosis and/or phagocytosis. Indeed, the macrophage-like phagocytic capacity of these amoabae is well documented and it was observed that *Dictyostelium* cells can internalize ferromagnetic particles 300 nm in diameter (Tatischeff, unpublished data). The observed decrease in cell flu-

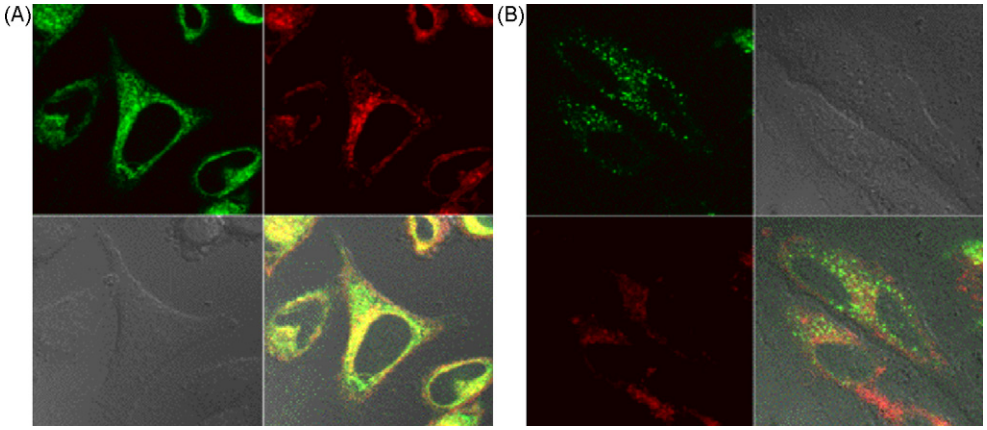

Fig. 7. Confocal microscopy images of hypericin within HeLa cells. (A) HeLa cells were incubated for 30 min in the presence of 7 µM hypericin packaged in nanovesicles. An additional 30 mn-period of incubation was carried out after addition of BODIPY FL C5-ceramide at 15 µM final concentration in DMEM. Hypericin is visualized in red and BODIPY in green. (B) HeLa cells were incubated for 60 min in the presence of both nanovesicles loaded with 7 µM hypericin and LysoTracker at 0.5 µM final concentration in DMEM. Hypericin is visualized in red and LysoTracker in green. All incubations were carried out in the dark at 37 °C in a humidified atmosphere with 5% CO_2.

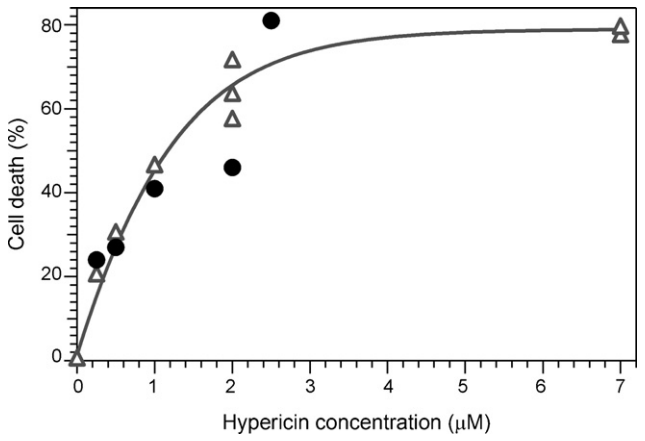

Fig. 8. Phototoxicity of free and vesicular hypericin on HeLa cells. Cell viability is measured by the MTT test. HeLa cells were seeded in a 96-well plate, incubated with hypericin and irradiated for 10 min using a 300 W Xenon arc light source (600 nm, 6.7 mW/cm^2). Maximum final concentration of vesicular hypericin was 2.5 μM, whereas free hypericin concentration reached 7 μM (see Section 2). Each point is the mean value of triplicates. Data were obtained in three independent experiments. (△) free hypericin; (●) vesicular hypericin.

orescence after a 48-h incubation time (Fig. 2B and C) probably originates from the observed vesicle-mediated release of hypericin. However, an intracellular accumulation of non-fluorescent hypericin aggregates might also be implied in the decrease. By subcellular time-resolved fluorescence spectroscopy, it was shown that tumor cells can internalize sensitizers in aggregated form and that aggregated species are present inside the cells (Kelbauskas and Dietel, 2002). The presence of hypericin aggregates within murine keratinocytes has also been reported (Theodossiou et al., 2004).

Photodynamic antitumoral therapy is based on the production by light absorbing molecules in the presence of oxygen, of cytotoxic reactive species, such as singlet oxygen, reported to diffuse on a limited distance during its excited state lifetime. As a consequence, the primary site of photodynamic action is closely linked to the location of the dye. As already mentioned for the free dye (Vandenbogaerde et al., 1998; Delaey et al., 2001), the present work indicates that hypericin, vectorized by the nanovesicles, accumulates in the Golgi perinuclear area of HeLa cells (Fig. 7). Moreover, we demonstrated that hypericin-loaded vesicles, in contrast with free hypericin dispersed in DMEM, allow significant *in vitro* internalization of hypericin in target cells without inducing cell damage by the observation light. The perinuclear Golgi location has been linked with the photodynamic efficiency of another photosensitizer, the Foscan®, in human HT29 colon carcinoma and MCF-7 breast carcinoma cell lines (Teiten et al., 2003). The photodynamic treatment of HeLa cells incubated in the presence of tetrabromorhodamine 123 induced damage in the Golgi apparatus, leading to calcium-dependent and caspase-3-independent apoptosis (Ogata et al., 2003). In the present work, vesicular-mediated delivery of hypericin depicts good photoefficiency for killing HeLa cells. The interest of using vesicular hypericin, instead of free hypericin, is a better control of drug cell loading, by an easy manipulation of the amount of vesicles incubated with the cells. Most importantly, the vesicular delivery prevents the detrimental aggregation of free hypericin in aqueous media.

Mammalian cell-derived exosomes are mostly considered as candidates to develop genetic vaccines for immunotherapy (Delcayre and Le Pecq, 2006). Bacterially derived particles, loaded with therapeutic drugs by a method equivalent to our «exogenous» encapsulation, have been shown to be efficient carriers (MacDiarmid et al., 2007). However, the problem of potential strong immunogenicity, due to their microbial origin may be a drawback for their use *in vivo*. By contrast, it has to be stressed that many proteins present in cell-derived exosomes are not detected in *Dictyostelium* nanovesicles. This should minimize the risk of undesirable immune responses upon *in vivo* administration, such as those triggered by tumor-released exosomes (Valenti et al., 2007). A first *in vivo* study upon the immunogenicity of *Dictyostelium* nanovesicles, intravenously injected twice in the tail of Balb/C mice, has shown a specific antibody response, but no pyrogenic response nor any inflammation, as measured by five pertinent cytokines (study performed by *Genosafe*, Evry, France).

5. Conclusion

Our work indicates that *D. discoideum* is a bio-engineering designer able to formulate vesicular drug carriers. To our knowledge, this is the first study describing cell-engineered vesicles able to load and vectorize a therapeutic molecule within human cells, as shown with the important photosensitizer, hypericin.

With regard to the possibility of using *Dictyostelium* nanovesicles in therapy, many problems remain to be solved. A study to elucidate the membrane events involved in cell entry of the drug vectorized by the nanovesicles should be performed. The previously detected lyso-bisphosphatidic acid (Tatischeff et al., 1998), whose fusogenic properties have been reported (Kobayashi et al., 2002) might be interesting, in this context. As a first *in vivo* approach, toxiciy and allergenic properties of the more purified vesicles are to be characterized. Taking into account the described culture of *Dictyostelium* cells in bioreactors (Lu et al., 2004), a vectorization strategy could be developed at a large scale. Such a vectorization strategy could be developed by using *Dictyostelium* cells cultured in the presence of magnetic nanoparticles (Wilhelm et al., 2008), oligonucleotides or antigenic peptides. Other characteristics of *Dictyostelium* vesicles appear interesting for targeting purpose; namely, the presence of discoidins I and II, which bind to the cell membrane with a specificity for galactose-related residues, might be of interest for lectin-mediated drug delivery (Bies et al., 2004). The targeting strategy tested with bacterially derived vesicles (MacDiarmid et al., 2007) using bispecific antibodies, with one arm recognizing a component of the vesicle surface, the other a cell-surface receptor of the target cell, might be applied to *Dictyostelium* vesicles.

Acknowledgements

We would like to thank Gilles Lemaitre (*i*stem, Evry, France) for help with the SDS-PAGE; Jean-Michel Guignet (CNRS UMR 7590, Paris, France) for measurements of the nanovesicle diameters and C. Lavialle (CNRS UMR 8122, Villejuif, France) for critical reading of the manuscript.

References

Agostinis, P., Vantieghem, A., Merlevede, W., de Witte, P.A., 2002. Hypericin in cancer treatment: more light on the way. Int. J. Biochem. Cell Biol. 34, 221–241.
Ajito, K., Torimitsu, K., 2002. Laser trapping and Raman spectroscopy of single cellular organelles in the nanometer range. Lab. Chip. 2, 11–14.
Alexander, S., Sydow, L.M., Wessels, D., Soll, D.R., 1992. Discoidin proteins of *Dictyostelium* are necessary for normal cytoskeletal organization and cellular morphology during aggregation. Differentiation 51, 149–161.
Bies, C., Lehr, C.M., Woodley, J.F., 2004. Lectin-mediated drug targeting: history and applications. Adv. Drug Deliv. Rev. 56, 425–435.
Blank, M., Mandel, M., Hazan, S., Keisari, Y., Lavie, G., 2001. Anti-cancer activities of hypericin in the dark. Photochem. Photobiol. 74, 120–125.
Boisset, N., Mouche, F., 2000. Sepia officinalis hemocyanin: a refined 3D structure from field emission gun cryoelectron microscopy. J. Mol. Biol. 296, 459–472.
Buytaert, E., Matroule, J.Y., Durinck, S., Close, P., Kocanova, S., Vandenheede, J.R., de Witte, P.A., Piette, J., Agostinis, P., 2008. Molecular effectors and modulators of hypericin-mediated cell death in bladder cancer cells. Oncogene 27, 1916–1929.
Cherney, D.P., Conboy, J.C., Harris, J.M., 2003. Optical-trapping Raman microscopy detection of single unilamellar lipid vesicles. Anal. Chem. 75, 6621–6628.

Delaey, E.M., Obermueller, R., Zupko, I., De Vos, D., Falk, H., de Witte, P.A., 2001. In vitro study of the photocytotoxicity of some hypericin analogs on different cell lines. Photochem. Photobiol. 74, 164–171.
Delcayre, A., Le Pecq, J.B., 2006. Exosomes as novel therapeutic nanodevices. Curr. Opin. Mol. Ther. 8, 31–38.
Deng, H., Bloomfield, V.A., Benevides, J.M., Thomas Jr., G.J., 1999. Dependence of the Raman signature of genomic B-DNA on nucleotide base sequence. Biopolymers 50, 656–666.
Derycke, A.S., De Witte, P.A., 2002. Transferrin-mediated targeting of hypericin embedded in sterically stabilized PEG-liposomes. Int. J. Oncol. 20, 181–187.
Dubochet, J., 2007. The physics of rapid cooling and its implications for cryoimmobilization of cells. Methods Cell Biol. 79, 7–21.
Galaz, S., Espada, J., Stockert, J.C., Pacheco, M., Sanz-Rodriguez, F., Arranz, R., Rello, S., Canete, M., Villanueva, A., Esteller, M., Juarranz, A., 2005. Loss of E-cadherin mediated cell–cell adhesion as an early trigger of apoptosis induced by photodynamic treatment. J. Cell Physiol. 205, 86–96.
Head, C.S., Luu, Q., Sercarz, J., Saxton, R., 2006. Photodynamic therapy and tumor imaging of hypericin-treated squamous cell carcinoma. World J. Surg. Oncol. 4, 87.
Heijnen, H.F., Schiel, A.E., Fijnheer, R., Geuze, H.J., Sixma, J.J., 1999. Activated platelets release two types of membrane vesicles: microvesicles by surface shedding and exosomes derived from exocytosis of multivesicular bodies and alpha-granules. Blood 94, 3791–3799.
Hugel, B., Martinez, M.C., Kunzelmann, C., Freyssinet, J.M., 2005. Membrane microparticles: two sides of the coin. Physiology (Bethesda) 20, 22–27.
Janssen, K.P., Rost, R., Eichinger, L., Schleicher, M., 2001. Characterization of CD36/LIMPII homologues in *Dictyostelium discoideum*. J. Biol. Chem. 276, 38899–38910.
Jonic, S., Sorzano, C.O., Cottevieille, M., Larquet, E., Boisset, N., 2007. A novel method for improvement of visualization of power spectra for sorting cryo-electron micrographs and their local areas. J. Struct. Biol. 157, 156–167.
Kelbauskas, L., Dietel, W., 2002. Internalization of aggregated photosensitizers by tumor cells: subcellular time-resolved fluorescence spectroscopy on derivatives of pyropheophorbide-a ethers and chlorin e6 under femtosecond one- and two-photon excitations. Photochem. Photobiol. 76, 686–694.
Kobayashi, T., Beuchat, M.H., Chevallier, J., Makino, A., Mayran, N., Escola, J.M., Lebrand, C., Cosson, P., Gruenberg, J., 2002. Separation and characterization of late endosomal membrane domains. J. Biol. Chem. 277, 32157–32164.
Krafft, C., Knetschke, T., Funk, R.H., Salzer, R., 2006. Studies on stress-induced changes at the subcellular level by Raman microspectroscopic mapping. Anal. Chem. 78, 4424–4429.
Kuronita, T., Eskelinen, E.L., Fujita, H., Saftig, P., Himeno, M., Tanaka, Y., 2002. A role for the lysosomal membrane protein LGP85 in the biogenesis and maintenance of endosomal and lysosomal morphology. J. Cell Sci. 115, 4117–4131.
Kuronita, T., Hatano, T., Furuyama, A., Hirota, Y., Masuyama, N., Saftig, P., Himeno, M., Fujita, H., Tanaka, Y., 2005. The NH(2)-terminal transmembrane and lumenal domains of LGP85 are needed for the formation of enlarged endosomes/lysosomes. Traffic 6, 895–906.
Laulagnier, K., Vincent-Schneider, H., Hamdi, S., Subra, C., Lankar, D., Record, M., 2005. Characterization of exosome subpopulations from RBL-2H3 cells using fluorescent lipids. Blood Cells Mol. Dis. 35, 116–121.
Lavialle, F., Levin, I.W., 1980. Raman spectroscopic study of the interactions of dimyristoyl- and 1-palmitoyl-2-oleoylphosphatidylcholine liposomes with myelin proteolipid apoprotein. Biochemistry 19, 6044–6050.
Lu, Y., Knol, J.C., Linskens, M.H., Friehs, K., Van Haastert, P.J., Flaschel, E., 2004. Production of the soluble human Fas ligand by *Dictyostelium discoideum* cultivated on a synthetic medium. J. Biotechnol. 108, 243–251.
MacDiarmid, J.A., Mugridge, N.B., Weiss, J.C., Phillips, L., Burn, A.L., Paulin, R.P., Haasdyk, J.E., Dickson, K.A., Brahmbhatt, V.N., Pattison, S.T., James, A.C., Al Bakri, G., Straw, R.C., Stillman, B., Graham, R.M., Brahmbhatt, H., 2007. Bacterially derived 400 nm particles for encapsulation and cancer cell targeting of chemotherapeutics. Cancer Cell 11, 431–445.
Marchetti, A., Mercanti, V., Cornillon, S., Alibaud, L., Charette, S.J., Cosson, P., 2004. Formation of multivesicular endosomes in *Dictyostelium*. J. Cell Sci. 117, 6053–6059.
Mathias, R.A., Lim, J.W., Ji, H., Simpson, R.J., 2009. Isolation of extracellular membranous vesicles for proteomic analysis. Methods Mol. Biol. 528, 227–242.
Neuhaus, E.M., Almers, W., Soldati, T., 2002. Morphology and dynamics of the endocytic pathway in *Dictyostelium discoideum*. Mol. Biol. Cell 13, 1390–1407.
Notingher, I., Verrier, S., Haque, S., Polak, J.M., Hench, L.L., 2003. Spectroscopic study of human lung epithelial cells (A549) in culture: living cells versus dead cells. Biopolymers 72, 230–240.
Ogata, M., Inanami, O., Nakajima, M., Nakajima, T., Hiraoka, W., Kuwabara, M., 2003. Ca(2+)-dependent and caspase-3-independent apoptosis caused by damage in Golgi apparatus due to 2,4,5,7 tetrabromorhodamine 123 bromide-induced photodynamic effects. Photochem. Photobiol. 78, 241–247.
Peterson, G.L., 1977. A simplification of the protein assay method of Lowry et al. which is more generally applicable. Anal. Biochem. 83, 346–356.
Ritz, R., Wein, H.T., Dietz, K., Schenk, M., Roser, F., Tatagiba, M., Strauss, W.S., 2007. Photodynamic therapy of malignant glioma with hypericin: comprehensive in vitro study in human glioblastoma cell lines. Int. J. Oncol. 30, 659–667.
Saw, C.L., Olivo, M., Soo, K.C., Heng, P.W., 2006. Delivery of hypericin for photodynamic applications. Cancer Lett. 241, 23–30.
Seitz, G., Krause, R., Fuchs, J., Heitmann, H., Armeanu, S., Ruck, P., Warmann, S.W., 2008. In vitro photodynamic therapy in pediatric epithelial liver tumors promoted by hypericin. Oncol. Rep. 20, 1277–1282.
Seitz, G., Warmann, S.W., Armeanu, S., Heitmann, H., Ruck, P., Hoffman, R.M., Fuchs, J., Wessels, J.T., 2007. In vitro photodynamic therapy of childhood rhabdomyosarcoma. Int. J. Oncol. 30, 615–620.
Simpson, R.J., Jensen, S.S., Lim, J.W., 2008. Proteomic profiling of exosomes: current perspectives. Proteomics 8, 4083–4099.
Stoorvogel, W., Kleijmeer, M.J., Geuze, H.J., Raposo, G., 2002. The biogenesis and functions of exosomes. Traffic 3, 321–330.
Sussman, M., 1987. Cultivation and synchronous morphogenesis of *Dictyostelium* under controlled experimental conditions. Methods Cell Biol. 28, 9–29.
Tatischeff, I., Bomsel, M., de Paillerets, C., Durand, H., Geny, B., Segretain, D., Turpin, E., Alfsen, A., 1998. *Dictyostelium discoideum* cells shed vesicles with associated DNA and vital stain Hoechst 33342. Cell. Mol. Life Sci. 54, 476–487.
Tatischeff, I., Lavialle, F., Pigaglio-Deshayes, S., Pechoux-Longin, C., Chinsky, L., Alfsen, A., 2008. *Dictyostelium* extracellular vesicles containing hoechst 33342 transfer the dye into the nuclei of living cells: a fluorescence study. J. Fluoresc. 18, 319–328.
Taylor, K.A., Glaeser, R.M., 1974. Electron diffraction of frozen, hydrated protein crystals. Science 186, 1036–1037.
Teiten, M.H., Bezdetnaya, L., Morliere, P., Santus, R., Guillemin, F., 2003. Endoplasmic reticulum and Golgi apparatus are the preferential sites of Foscan localisation in cultured tumour cells. Br. J. Cancer 88, 146–152.
Theodossiou, T., Spiro, M.D., Jacobson, J., Hothersall, J.S., Macrobert, A.J., 2004. Evidence for intracellular aggregation of hypericin and the impact on its photocytotoxicity in PAM 212 murine keratinocytes. Photochem. Photobiol. 80, 438–443.
Thery, C., Zitvogel, L., Amigorena, S., 2002. Exosomes: composition, biogenesis and function. Nat. Rev. Immunol. 2, 569–579.
Torchilin, V.P., 2005. Recent advances with liposomes as pharmaceutical carriers. Nat. Rev. Drug Discov. 4, 145–160.
Uzdensky, A.B., Bragin, D.E., Kolosov, M.S., Kubin, A., Loew, H.G., Moan, J., 2003. Photodynamic effect of hypericin and a water-soluble derivative on isolated crayfish neuron and surrounding glial cells. J. Photochem. Photobiol. B 72, 27–33.
Uzunbajakava, N., Lenferink, A., Kraan, Y., Willekens, B., Vrensen, G., Greve, J., Otto, C., 2003. Nonresonant Raman imaging of protein distribution in single human cells. Biopolymers 72, 1–9.
Valenti, R., Huber, V., Iero, M., Filipazzi, P., Parmiani, G., Rivoltini, L., 2007. Tumor-released microvesicles as vehicles of immunosuppression. Cancer Res. 67, 2912–2915.
Van De Putte, M., Roskams, T., Bormans, G., Verbruggen, A., De Witte, P.A., 2006. The impact of aggregation on the biodistribution of hypericin. Int. J. Oncol. 28, 655–660.
van Niel, G., Raposo, G., Candalh, C., Boussac, M., Hershberg, R., Cerf-Bensussan, N., Heyman, M., 2001. Intestinal epithelial cells secrete exosome-like vesicles. Gastroenterology 121, 337–349.
Vandenbogaerde, A.L., Delaey, E.M., Vantieghem, A.M., Himpens, B.E., Merlevede, W.J., de Witte, P.A., 1998. Cytotoxicity and antiproliferative effect of hypericin and derivatives after photosensitization. Photochem. Photobiol. 67, 119–125.
Weissig, V., Boddapati, S.V., Cheng, S.M., D'Souza, G.G., 2006. Liposomes and liposome-like vesicles for drug and DNA delivery to mitochondria. J. Liposome Res. 16, 249–264.
Wielgus, A.R., Chignell, C.F., Miller, D.S., Van Houten, B., Meyer, J., Hu, D.N., Roberts, J.E., 2007. Phototoxicity in human retinal pigment epithelial cells promoted by hypericin, a component of St. John's wort. Photochem. Photobiol. 83, 706–713.
Wilhelm, C., Lavialle, F., Pechoux, C., Tatischeff, I., Gazeau, F., 2008. Intracellular trafficking of magnetic nanoparticles to design multifunctional biovesicles. Small 4, 577–582.
Wubbolts, R., Leckie, R.S., Veenhuizen, P.T., Schwarzmann, G., Mobius, W., Hoernschemeyer, J., Slot, J.W., Geuze, H.J., Stoorvogel, W., 2003. Proteomic and biochemical analyses of human B cell-derived exosomes. Potential implications for their function and multivesicular body formation. J. Biol. Chem. 278, 10963–10972.
Yorikawa, C., Shibata, H., Waguri, S., Hatta, K., Horii, M., Katoh, K., Kobayashi, T., Uchiyama, Y., Maki, M., 2005. Human CHMP6, a myristoylated ESCRT-III protein, interacts directly with an ESCRT-II component EAP20 and regulates endosomal cargo sorting. Biochem. J. 387, 17–26.
Zhang, W., Lawa, R.E., Hintona, D.R., Su, Y., Couldwell, W.T., 1995. Growth inhibition and apoptosis in human neuroblastoma SK–N–SH cells induced by hypericin, a potent inhibitor of protein kinase C. Cancer Lett. 96, 31–35.